

# SAR Speckle Nonlocal Filtering With Statistical Modeling of Haar Wavelet Coefficients and Stochastic Distances

Pedro A. A. Penna<sup>✉</sup>, Student Member, IEEE, and Nelson D. A. Mascarenhas, Life Senior Member, IEEE

**Abstract**—Due to the coherent processing of synthetic aperture radar (SAR) systems, multiplicative speckle noise arises providing a granular appearance in SAR images. This kind of noise makes it difficult to analyze and interpret surface images from the earth. Therefore, studying alternatives to attenuate the speckle is a constant task in the image processing literature. Current state-of-the-art filters in remote sensing area explore the philosophy of similarity between patches. This paper aims to expand the traditional nonlocal means (NLM) algorithm originally proposed for the additive white Gaussian noise (AWGN) to deal with the speckle. In our research, we consider the worst scenario, i.e., the single-look speckle noise, and apply the NLM to filter intensity SAR images in the Haar wavelet domain. To accomplish this task, the Haar coefficients were described by exponential-polynomial (EP) and gamma distributions. Furthermore, stochastic distances based on these two mentioned distributions were derived and embedded in the NLM filter by replacing the Euclidean distance of the original method. This represents the main contribution of the proposed research. Finally, this paper analyzes and compares the synthetic and real experiments of the proposed method with some recent filters of the literature demonstrating its competitive performance.

**Index Terms**—Denoising, exponential-polynomial (EP) distribution, Haar wavelet, nonlocal means (NLM) algorithm, synthetic aperture radar (SAR) image, speckle noise, stochastic distances.

## I. INTRODUCTION

IMAGE denoising filters may be applicable to a vast amount of disciplines, such as medicine, forensic science, astronomy, biology, and others [1]. For this reason, the image processing literature extensively searches for new algorithms to attenuate noise and to extend already proposed techniques [2].

Manuscript received September 3, 2018; revised January 24, 2019 and March 27, 2019; accepted April 10, 2019. Date of publication May 14, 2019; date of current version August 27, 2019. This work was supported in part by the Coordenação de Aperfeiçoamento de Pessoal de Nível Superior (CAPES), Brazil, under Grant 001. The work of P. A. A. Penna was supported by the CAPES Scholarship. The work of N. D. A. Mascarenhas was supported by CNPq, Brazil, through a scholarship under Grant 306742/2017-9. (*Corresponding author: Pedro A. A. Penna.*)

P. A. A. Penna is with the Computing Department, Federal University of São Carlos (UFSCar), 13565-905 São Carlos, Brazil (e-mail: pedro.penna@dc.ufscar.br).

N. D. A. Mascarenhas is with the Computing Department, Federal University of São Carlos (UFSCar), 13565-905 São Carlos, Brazil, and also with the Centro Universitário Campo Limpo Paulista (UNIFACCAMP), Campo Limpo Paulista 13231-220, Brazil (e-mail: nelson@dc.ufscar.br).

Color versions of one or more of the figures in this article are available online at <http://ieeexplore.ieee.org>.

Digital Object Identifier 10.1109/TGRS.2019.2912153

Synthetic aperture radar (SAR) systems are very useful for monitoring and studying the earth's surface, such as oil leakage in the oceans, melting glaciers, borderlands analysis, and so on. The main advantage of this kind of system is its applicability in all sunlight and weather conditions [3]. Nevertheless, the resulting images of the coherent processing are contaminated with multiplicative speckle noise that emerges from the interference on the echo given by the surface elements of the target [4]. The speckle gives a granular appearance in SAR images, making their analyses and interpretations a difficult task with high chances of errors.

However, speckle is noisy due to the fact that it carries information about the target [5]. In addition, SAR images with speckle should not be processed with filters based on the additive white Gaussian noise (AWGN) concept, because the speckle corrupts the return signal in a multiplicative way, i.e., the noise distribution is not Gaussian. There is an argument for the use of the multilook technique, but it reduces the noise at the cost of resolution loss. Therefore, it is of great importance to study alternatives to mitigate speckle noise [6].

Some techniques present in the image processing literature, for example, homomorphic transformation [7], make the AWGN filters capable of filtering speckle; a noise present not only in SAR images, but also in medical ultrasound, sonar, and laser images.

The nonlocal means (NLM) approach [8] changed the course of image noise attenuation literature and it provided the basis for the collaborative filtering techniques such as block-matching 3-D (BM3D) [9] and sparsity-based methods such as K-SVD [10]. The cornerstone of these techniques is the assumption of similarity between patches, i.e.,  $n \times n$  windows with  $n \in \mathbb{N}^*$  and odd, centered in the pixels of an image [4] first proposed in [11]. The similarity between two patches is provided by a metric that relates the gray values of the pixels inside each patch.

The NLM and BM3D filters, as well as a plethora of other methods, were originally proposed for AWGN noise. Developing techniques capable of removing different kinds of noise is very important. The probabilistic patch-based (PPB) filter [12] works with additive and multiplicative noise. Also, it is possible to apply different similarity measures replacing the Euclidean distance of the NLM algorithm as in [13]. The NLM technique was also applied to reduce speckle noise in (Pol)(In)SAR images [14] and in methods that use the physical characteristics of the imaged targets [15]. Recent studies also

used the NLM with total variation regularization to attenuate the speckle [16]. Regarding the SAR image, SAR-BM3D [5] and FANS [17] are considered the state of the art with very good results [4]. The SAR-BM3D filter uses the BM3D philosophy, which is also a patch-based technique. It is a filter with a more advanced method. One of the objectives of this paper is to explore a way to use a filter originally developed for the spatial domain in the wavelet domain. This is possible through the stochastic distances.

There is another line of study that adapts divergence measures to deal with image processing tasks [18]. The stochastic distance concept has been studied for different types of noise and images. These distances have already been used to remove speckle in SAR images [4], [19]–[21] and ultrasound images [22]–[24]. Also, in [25] and [26], the distances were used to filter Poisson noise.

Under the concept of wavelets [27], we can say that the Haar wavelet is the simplest case [28]. The wavelet transform paradigm has been adopted by a large number of applications in many areas, such as astrophysics, geophysics, geoprocessing, and medicine [29]. This paper is designed for Haar wavelet due to the analytical tractability of the coefficients obtained with this wavelet. The objective is to apply the NLM filter in the wavelet domain to attenuate the speckle noise in intensity SAR images. The main contribution of this paper is to present new stochastic distances based on the gamma and exponential-polynomial (EP) distributions [30]. These distances are inserted into the filter making it suitable for filtering speckle noise in the wavelet domain.

Finally, this paper exposes the results of both synthetic and real scenarios to show that the proposed method and distances generate good results that are competitive with the state-of-the-art filters. It also presents the results of classical speckle filters, such as Lee [31], Frost [32], and NURW [33]. Furthermore, other NLM-based algorithms are also compared.

The rest of this paper is organized as follows. Section II presents the model of speckle. The wavelets' fundamentals and the EP distribution are discussed in Section III. Section IV explains the NLM filter and the stochastic distances for EP and gamma distributions. Real and synthetic experiments are discussed in Section V and the proposed research is concluded with future works in Section VI.

## II. MODEL OF SPECKLE FOR SAR INTENSITY IMAGE

An SAR system sends electromagnetic pulses and captures the backscattered echo of an area (“resolution cell”). Considering an intensity SAR image, the return  $Z$  is the product of two independent random variables given by

$$Z = X \cdot Y \quad (1)$$

where  $X$  and  $Y$  represent, respectively, the backscatter return and the speckle noise.

The echo signal is by nature complex-valued and it can be seen as a summation of the return of several backscattered objects [6]. Additionally, only the amplitude value is informative [3]. The square of the amplitude, i.e., the intensity format follows a Gamma distribution

$f_Y(y) \sim \Gamma(L, L/\alpha)$  [7], [34] with a probability density function (pdf), is expressed by [30]

$$f_Y(y; L, L/\alpha) = \frac{L^L}{\alpha \Gamma(L)} \left(\frac{y}{\alpha}\right)^{L-1} \exp\left(-\frac{L}{\alpha}y\right) \quad (2)$$

where  $L > 0$  and  $\alpha$  denote, respectively, the number of looks and the underlying reflectivity mean.

## III. HAAR WAVELET DOMAIN: THE EP DISTRIBUTION

In the image processing area, the wavelet theory has been widely used because of the advantage of time–frequency and multiscale analyses [35]. A denoising method with wavelets tends to be superior to other approaches when the noise is AWGN. However, the use of wavelets to attenuate speckle has not yet produced desirable results, since the speckle remains in the low-pass component, i.e., the approximation component obtained with the wavelet scale function [35]. Therefore, there is a great interest in research involving filtering SAR images with wavelets. A wavelet can be expressed by

$$\psi_{a,b}(t) = \frac{1}{\sqrt{a}} \psi\left(\frac{t-b}{a}\right) \quad (3)$$

where  $a$  corresponds to the scale size, i.e., contraction or dilation, while  $b$  is responsible for the translation (displacement) and  $t$  denotes time.

The wavelet format will remain the same under the translation and scaling process. The wavelet coefficients are the components of the signal with the wavelet at different scales and locations along the 1-D axis [30].

The signal  $x$  can be decomposed by the expression [36]

$$x(t) = \sum_{k=-\infty}^{\infty} c_{j,k} \phi_{j,t}(k) + \sum_{k=-\infty}^{\infty} \sum_{j=1}^J \psi_{j,t}(k) w_{j,k} \quad (4)$$

where

$$\phi_{j,t}(x) = 2^{-j} \phi(2^{-j}x - t) \quad (5)$$

and

$$\psi_{j,t}(x) = 2^{-j} \psi(2^{-j}x - t). \quad (6)$$

The  $\phi$  function denotes the scale function and  $\psi$  represents the wavelet. The  $j$  parameter indicates the number of resolutions for decomposition. This decomposition consists of two discrete convolutions [discrete wavelet transform (DWT)] followed by a subsampling by 2. The coefficients are expressed by

$$c_{j+1,t} = \sum_{k=-\infty}^{\infty} h(k-2t) c_{j,k} \quad (7)$$

$$w_{j+1,t} = \sum_{k=-\infty}^{\infty} g(k-2t) c_{j,k}. \quad (8)$$

$w_{j,t}$  is the wavelet coefficient, i.e., it represents the signal details at scale  $j$ . The  $c_{j,t}$  coefficient represents a smoothed version of the original signal from the scale function.

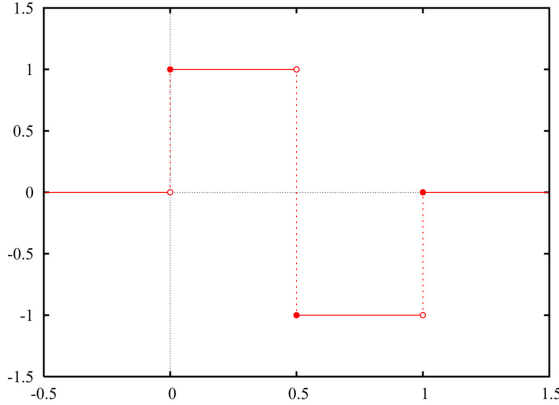


Fig. 1. Haar wavelet.

The  $h$  and  $g$  terms represent, respectively, the low-pass and high-pass impulse response of the filters given by

$$\frac{1}{2}\phi\left(\frac{x}{2}\right) = \sum_{k=-\infty}^{\infty} h(k)\phi(x-k) \quad (9)$$

$$\frac{1}{2}\psi\left(\frac{x}{2}\right) = \sum_{k=-\infty}^{\infty} g(k)\psi(x-k). \quad (10)$$

#### A. Haar Wavelet

The Hungarian mathematician Alfred Haar developed the Haar wavelet around 1910 [28]. This wavelet was the first, and therefore the simplest, example of an orthonormal wavelet transformation. The Haar function  $\psi(t)$  is a rectangular pulse [28] and it can be described as

$$\psi(t) = \begin{cases} 1 & 0 \leq t < \frac{1}{2} \\ -1 & \frac{1}{2} \leq t < 1 \\ 0 & \text{otherwise.} \end{cases} \quad (11)$$

Fig. 1 shows the Haar wavelet  $\psi$ . The scale function  $\phi(t)$  is given by

$$\phi(t) = \begin{cases} 1 & 0 \leq t < 1 \\ 0 & \text{otherwise.} \end{cases} \quad (12)$$

#### B. EP Distribution

The EP distribution [30] has emerged for the Haar wavelet coefficients. The EP distribution describes the difference between two independent random variables fitted by the gamma distribution, which, for single-look SAR images ( $L = 1$ ), is an exponential distribution, i.e., the EP pdf is a gamma convolved with the same gamma, but with the inverted argument [37]. Moreover, since the gamma distribution is an exponential for  $L = 1$ , the difference between two gammas can be defined as a generalization of the Laplace distribution, which is the difference of two exponentials [38]. Fig. 2 shows the graphs of the wavelet coefficients with the EP distribution,

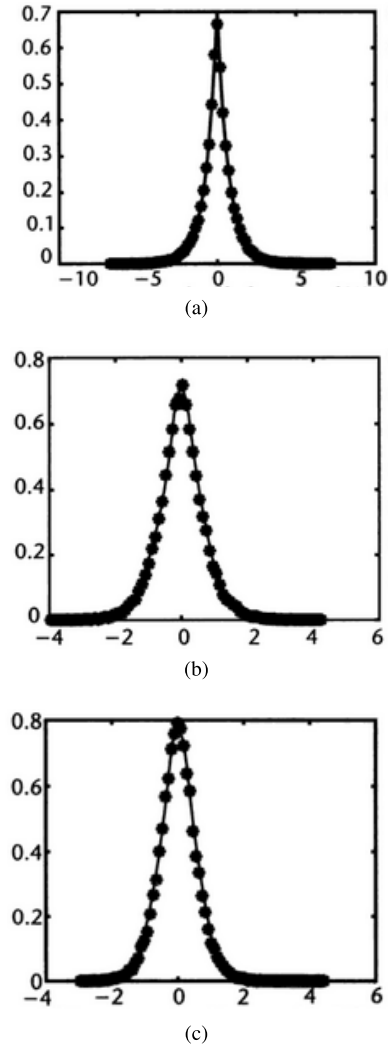


Fig. 2. Pdf of EP for different looks considering one decomposition level with the Haar wavelet. (a) Single look. (b) Three looks. (c) Four looks.

considering one decomposition level with the Haar wavelet. The expression for the EP distribution is given by

$$p_{\text{ep}}(y) = \frac{\exp\left(-\frac{L}{b}|y|\right)}{(L-1)!} \left(\frac{L}{a}\right)^L \left(\frac{L}{b}\right)^L \times \left[ \sum_{j=0}^{L-1} \frac{(L+j-1)!}{j!(L-j-1)!(\frac{L}{a}+\frac{L}{b})^{L+j}} |y|^{L-j-1} \right] \quad (13)$$

where  $a$  and  $b$  are the mean values of two different patches considering the NLM paradigm. It is called EP because  $p_{\text{ep}}(y)$  is a product of an exponential function by a polynomial function. If a random variable follows the EP distribution, it is defined as  $x \sim EP(L, L/a, L/b)$ .

Through the Haar wavelet with an  $M$  decomposition level, the scale  $c^M$  and detail  $w^M$  coefficients extracted from an SAR image can be fitted by (14) and (15) [30]

$$c^M \sim \Gamma(4^M L, 2^{-M}) \quad (14)$$

$$w^M \sim EP(2^{2M-1} L, 2^{-M} L). \quad (15)$$

#### IV. NONLOCAL MEANS AND STOCHASTIC DISTANCES

This section presents the stochastic distances formulated to remove the most aggressive speckle noise, i.e., the single-look case, in the wavelet domain. The statistical properties of the noise are considered constant throughout the image.

The nonlocality paradigm exposed by the NLM [8] algorithm acts with the patches' similarity of an image. Patches are windows of  $m \times m$  size centered in certain pixels. The NLM will compute a weighted average distance between the patches with the weights calculated by the Euclidean distance [4].

Considering AWGN noise  $n$  with zero mean and variance  $\sigma^2$  and given an image  $x$  corrupted by  $n$ , the  $i$ th noisy pixel is expressed by  $y_i = x_i + n_i$ . The weighted average is applied for each pixel at the search area  $S_i$  to estimate the noise free image

$$\hat{x}_i = \frac{\sum_{j \in S_i} w_{i,j} y_j}{\sum_{j \in S_i} w_{i,j}}. \quad (16)$$

The weight  $w_{i,j}$  gives the similarity between the patches centered at pixels  $i$  and  $j$ . It is computed by the expression  $w_{i,j} = e^{-d_{i,j}/h^2}$ , where  $d_{i,j} = \|P_i - P_j\|_2^2$  is the Euclidean distance of the vectorized patches  $P_i$  and  $P_j$  and  $h$  is the smoothing parameter.

In [18], the family of divergences  $(h, \phi)$  [39] was used to derive the stochastic distance integrals: Kullback–Leibler, Rényi, Hellinger, Bhattacharyya, Jensen–Shannon, Arithmetic–Geometric, Triangular, and Harmonic Mean.

Based on the integrals of the stochastic distances, the new distances for the EP distribution were computed using the MATLAB R2016a [40] software. In (17)–(24),  $a_1$  and  $a_2$  represent the means of two different patches. The original Euclidean distance of the NLM filter was replaced by these new distances.

##### Kullback–Leibler Distance ( $d_{KLEP}$ ):

$$d_{KLEP} = \frac{(\ln(a_1 + 1) - \ln(a_2 + 1))(a_1 - a_2)}{2(a_1 + 1)(a_2 + 1)}. \quad (17)$$

##### Hellinger Distance ( $d_{HEP}$ ):

$$d_{HEP} = \frac{a_1 + a_2 - 2\sqrt{a_1 + 1}\sqrt{a_2 + 1} + 2}{(2a_1 + 2)(a_2 + 1)}. \quad (18)$$

##### Rényi Distance With $\beta = 0.5$ ( $d_{REP}$ ):

$$d_{REP} = -2\ln(1 - d_H). \quad (19)$$

##### Bhattacharyya Distance ( $d_{BEP}$ ):

$$d_{BEP} = -\ln(1 - d_H). \quad (20)$$

##### Jensen–Shannon ( $d_{JSEP}$ ):

$$d_{JSEP} = \frac{(\ln(2a_2 + 2) - \ln(a_1 + a_2 + 2))}{2(a_1 + 1)} + \frac{(\ln(2a_1 + 2) - \ln(a_1 + a_2 + 2))}{2(a_2 + 1)}. \quad (21)$$

##### Arithmetic–Geometric Distance ( $d_{AGEP}$ ):

$$d_{AGEP} = \frac{(\ln(a_2 + 1) + \ln(4a_1 + 4) - 2\ln(a_1 + a_2 + 2))(a_1 + a_2 + 2)}{4(a_1 + 1)(a_2 + 1)}. \quad (22)$$

##### Triangular Distance ( $d_{TEP}$ ):

$$d_{TEP} = \frac{(a_1 - a_2)^2}{(a_1 + 1)(a_2 + 1)(a_1 + a_2 + 2)}. \quad (23)$$

##### Harmonic-Mean Distance ( $d_{HMEP}$ ):

$$d_{HMEP} = -\ln\left(1 - \frac{d_T}{2}\right). \quad (24)$$

According to (14), it is known that the approximation coefficient of an SAR image follows a gamma distribution when a wavelet decomposition appears. Therefore, the distances for this distribution were also computed. However, for the eight stochastic distances in [18], only four distances had their closed formulas found by (25)–(28).

##### Kullback–Leibler Distance ( $d_{KLG}$ ):

$$d_{KLG} = \frac{(a_1 - a_2)^2}{2a_1 a_2}. \quad (25)$$

##### Hellinger Distance ( $d_{HG}$ ):

$$d_{HG} = \frac{(\sqrt{a_1} - \sqrt{a_2})^2}{a_1 + a_2}. \quad (26)$$

##### Rényi Distance With $\beta = 0.5$ ( $d_{RG}$ ):

$$d_{RG} = -2\ln\left(\frac{2\sqrt{a_1}\sqrt{a_2}}{a_1 + a_2}\right). \quad (27)$$

##### Bhattacharyya Distance ( $d_{BG}$ ):

$$d_{BG} = -\ln\left(\frac{2\sqrt{a_1}\sqrt{a_2}}{a_1 + a_2}\right). \quad (28)$$

#### A. Distances Properties

A distance  $d(i, j)$ , with  $i \in R$  and  $j \in R$ , must be as follows:

- 1) homogeneous [ $d(i, i) = 0$ ];
- 2) symmetrical [ $d(i, j) = d(j, i)$ ];
- 3) positive [ $d(i, j) > 0, i \neq j$ ].

Observing Figs. 3 and 4, it is possible to visualize the good behavior of the stochastic distances obtained for the EP and gamma distributions considering single-look speckle. These figures show a 3-D plot in a grid, where the values of the averages used in the distances were in an interval between 0 and 255. The interval was randomly chosen and it is believed that the behavior of the graphs is the same for a longer interval. For both distributions, the plots are above the x-axis. The dark blue color indicates the zero value when  $x$  and  $y$  are equal and it is possible to see the symmetry of the curves when interchanging  $x$  and  $y$  values.

#### V. RESULTS AND DISCUSSION

Fig. 5 shows the diagram of the proposed method. First, the noisy image, i.e., the return  $Z$  of (1), is decomposed with one level using the Haar wavelet. Therefore, we have the approximation (scale) coefficient (ac) and the details' coefficients: horizontal (Hc), vertical (Vc), and diagonal (dc). Note that L indicates the low-pass filter, while H denotes the high-pass filter. We chose to work with only one level of decomposition because, experimentally, using more levels

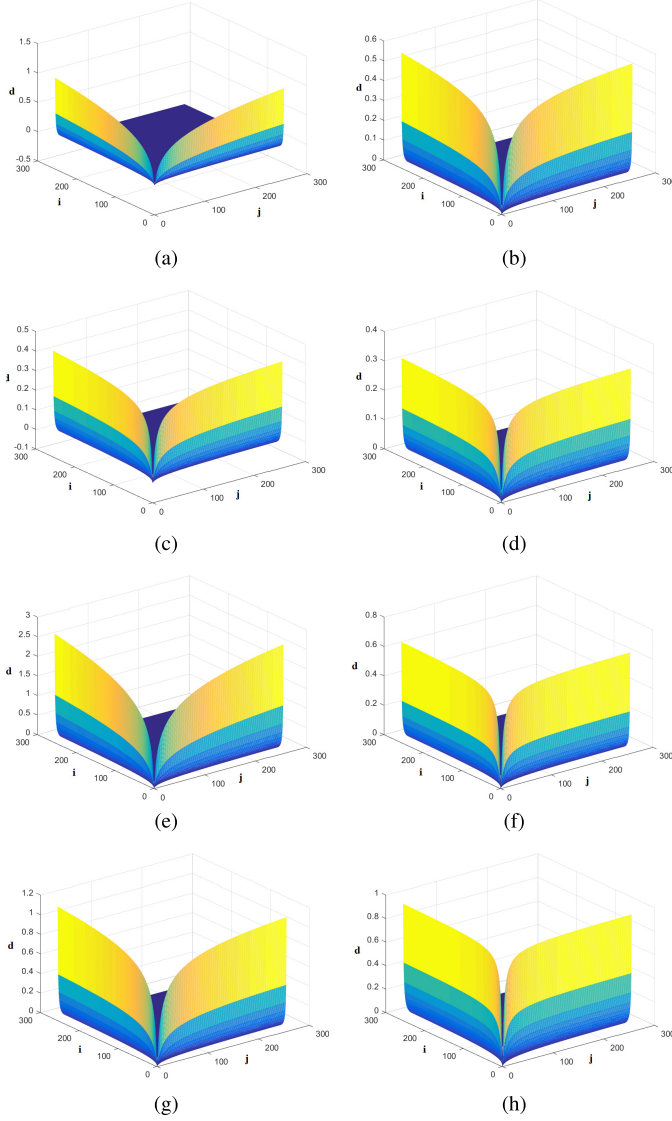


Fig. 3. Stochastic distance 3-D plots for the EP distribution for single-look speckle. (a) Arithmetic-geometric. (b) Bhattacharyya. (c) Hellinger. (d) Jensen-Shannon. (e) Kullback-Leibler. (f) Harmonic-mean. (g) Rényi. (h) Triangular.

did not result in a better filtered image. Finally, after the NLM filtering with the stochastic distances for gamma and EP distributions, an inverse DWT (IDWT) is performed to obtain the filtered image.

To compare the proposed filter, the following algorithms with the available codes were used: FANS [17], OBNLM [41], Iterative PPB [12], SAR-BM3D [5], Lee [31], Frost [32], NURW [33], FNLM [42], PNLM [43], and NLM-SAP [44]. It is important to note that, for the methods based on the NLM approach originally developed to attenuate the AWGN, we used the homomorphic transformation [7]. Furthermore, for the mentioned algorithms, we chose the parameter settings proposed in the original papers.

For the real and synthetic experiments in the following, the following stochastic distances were used: Kullback-Leibler for NLM with gamma distribution and Jensen-Shannon for NLM with EP distribution. These distances were chosen for

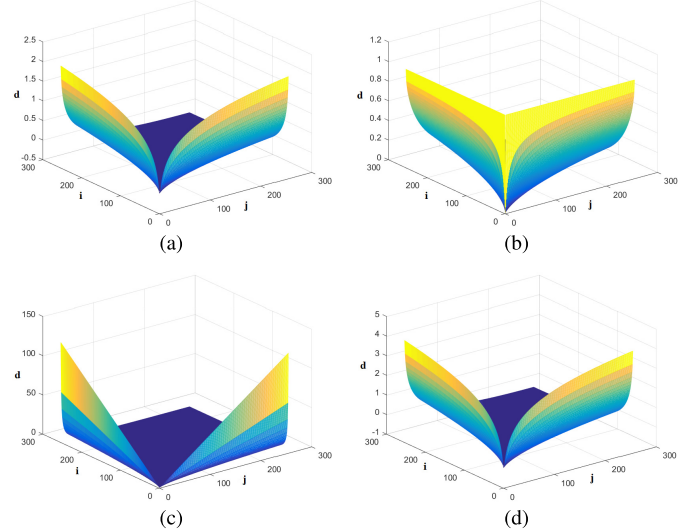


Fig. 4. Stochastic distances 3-D plots for the gamma distribution for single-look speckle. (a) Bhattacharyya. (b) Hellinger. (c) Kullback-Leibler. (d) Rényi.

two reasons. The first reason is that the stochastic distances provided very close results in the work [4]. In addition, we believe that choosing different distances for the approximation and detail coefficients will have no detrimental effect on the final filtering result since the denoising steps occur in isolated processes according to Fig. 5.

#### A. Synthetic Experiments

For the synthetic experiments, four cases of the SAR Benchmark Framework [45] were used: building, corner, homogeneous, and squares. The first three images have  $256 \times 256$  dimension and the last one has  $512 \times 512$ . For each image, eight speckle realizations were performed. Therefore, all the measures presented in the following tables were based on the average of the eight corrupted images. We recommend accessing the full paper [45] for more information about these images. Fig. 6 shows the original and corrupted images with the single-look speckle noise.

Any filter forged by the NLM paradigm needs to be set with three basic parameters: search window, patches sizes, and smoothing parameter  $h$ . Table I shows the parameters' definition for each image. All values were found experimentally. The scale coefficient is represented by  $c$  while the detail coefficient is denoted by  $w$ . According to [4], there is not a known and closed formula in the literature to compute an ideal value for the  $h$  parameter. The values for the other filters used for comparison were configured with the default values described by the respective papers.

1) *Homogeneous*: For this image, we use the mean value (MoF) of the filtered image  $\hat{f}$  and the mean (MoR) and variance (VoR) values of the ratio image ( $r = Z/\hat{f}$ ). The MoF, MoR, and VoR values are useful to assess the radiometric preservation by comparing the local mean backscattering reflectivity values in the original and filtered images [45]. If the mean intensity was not significantly altered, it could mean that the filter provided a good speckle reduction and did

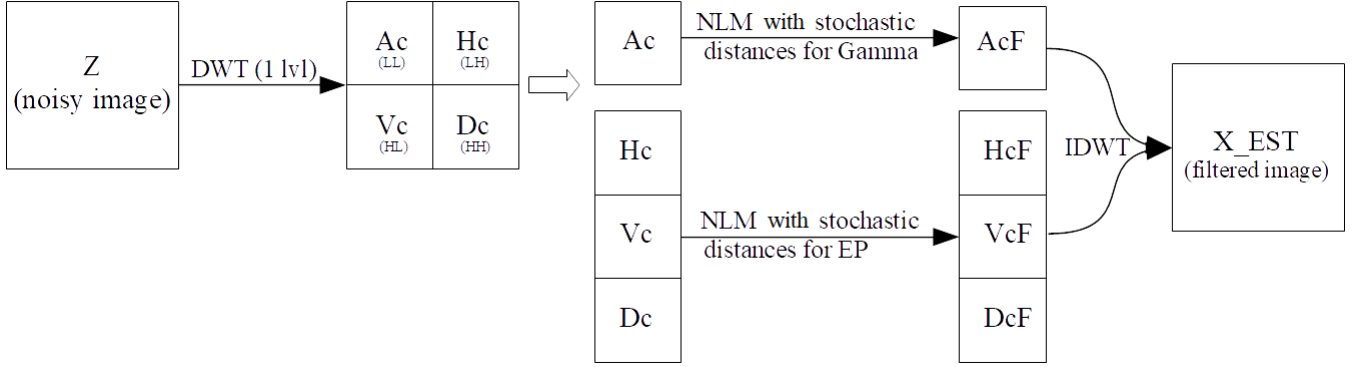


Fig. 5. Diagram of the proposed method with one-level decomposition using the Haar wavelet.

TABLE I  
PARAMETERS' CONFIGURATION FOR SYNTHETIC EXPERIMENTS

Image	$h$ for $c$	$h$ for $w$	Patch size $c$	Patch size $w$	Search area size $c$	Search area size $w$
Homogeneous	0.22	$3.75 \times \sigma_c$	$5 \times 5$	$5 \times 5$	$15 \times 15$	$15 \times 15$
Squares	0.22	$20.35 \times \sigma_c$	$5 \times 5$	$5 \times 5$	$11 \times 11$	$11 \times 11$
Corner	0.22	$1.35 \times \sigma_c$	$3 \times 3$	$3 \times 3$	$7 \times 7$	$7 \times 7$
Building	$5 \times 10^{-3}$	$0.92 \times \sigma_c$	$3 \times 3$	$3 \times 3$	$19 \times 19$	$19 \times 19$

not cause severe radiometric distortions. Also, the ratio image should only present the speckle pattern, i.e.,  $MoR \approx 1$  and  $VoR \approx 1/L$  [45]. A  $VoR < 1$  case means undersmoothing, i.e., some speckle remains in the filtered image, whereas  $VoR > 1$  suggests oversmoothing, i.e., some details of the filtered image are lost.

The  $ENL = \mu_Z^2/\sigma_Z^2$  tool, where  $\mu_Z$  and  $\sigma_Z^2$  are, respectively, the local mean and local variance of a homogeneous region, is used very much in the literature to measure speckle attenuation [45]. A larger ENL value means a better speckle mitigation. However, the ENL favors oversmoothed image [4].

Since, within the synthetic experiment, we have the original noise free image, it is possible to apply the despeckling gain measure (DG) [45] expressed by

$$DG = 10 \log_{10}(MSE(X, Z)/MSE(X, \hat{f})) \quad (29)$$

with

$$MSE(X, \hat{f}) = \frac{1}{\text{size}(X)} \sum_{i,j} (X(i, j) - \hat{f}(i, j))^2. \quad (30)$$

Larger values for the DG measure indicate better speckle suppression.

In Table II, we present the MoF, MoR, VoR, ENL, and DG values. The time in seconds for each filter processing has also been added. PM denotes the proposed method. Fig. 7 shows the results of the filters applied to the homogeneous image. Since the ratio images are not informative for this case [45], they are not shown. All filters' results provided a mean value close to the ideal value and VoR is smaller than one except for PNLM. The proposed method obtained better values than the classical and the other NLM-based filters. Moreover, the ENL and DG values of the proposed approach were better than SAR-BM3D. The FANS algorithm presented the best values for ENL and DG measures although the PM value for DG

TABLE II  
VALUES FOR HOMOGENEOUS IMAGE. PM: PROPOSED METHOD. VALUES ARE AVERAGES OVER EIGHT SPECKLE REALIZATIONS

	MoF	MoR	VoR	ENL	DG	Time (s)
Clean	1.00	0.99	0.98	436.97	-	-
Noisy	0.99	-	-	1.00	0	-
FANS	1.00	0.98	0.93	144.69	20.48	2.55
OBNL	0.98	0.93	0.59	20.66	13.13	0.34
PM	0.99	0.99	0.96	136.79	20.45	69.92
PPB	0.99	0.96	0.82	127.68	20.19	22.27
SAR-BM3D	0.97	0.97	0.81	102.44	19.40	32.47
Lee	0.99	0.99	0.73	7.03	8.40	0.00
Frost	0.99	0.90	0.45	9.67	9.79	0.89
NURW	0.99	0.99	0.96	189.68	21.58	0.02
FNLM	1.28	0.62	0.13	4.02	3.09	0.17
NLM-SAP	1.01	0.98	0.96	56.42	16.96	10.80
PNLM	0.98	1.06	1.16	60.56	17.38	8.69

is very close. It is possible to note that the NURW, PNLM, and NLM-SAP values are larger for some measures, but their images are noisy or blurred. Visually, it is possible to see that the PPB tends to produce a highly blurred image and the OBNLM image still has strong speckle residue. The PM algorithm provides an image with superior visual than PPB with a less blurry image. Although artifacts can also be found due to the wavelet-based technique, the image is better than the OBNLM. In general, by analyzing the filtered images, it can be said that the results follow the values in Table II.

2) Squares: The second case is formed by four areas with different mean intensity values. In this scenario, the objective is to evaluate the edges' degradation after filtering. The edge smearing (ES) and Pratt's FOM [45] are measures that estimate when the edges are still recognizable after the filtering process.

ES is the weighted square error between the edge profiles of the filtered ( $EP_{\hat{f}}$ ) and the reference image ( $EP_X$ ) expressed

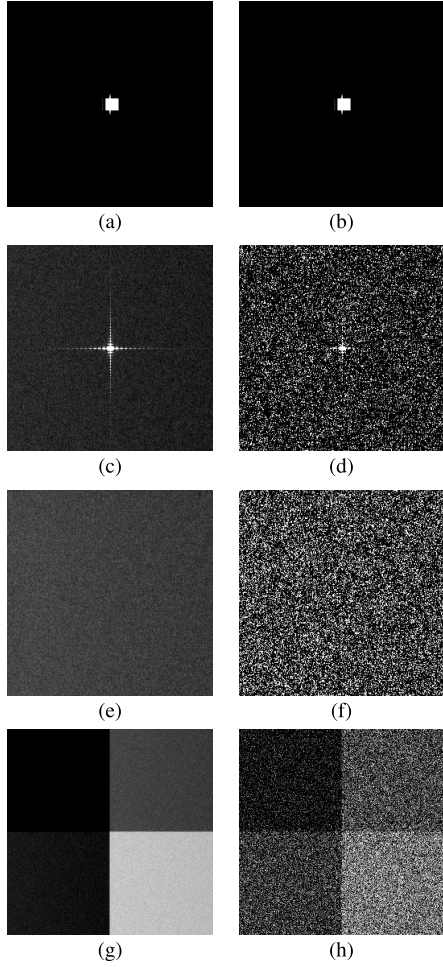


Fig. 6. Single-look speckle noise for the synthetic experiments. (a) Building. (b) Noisy building. (c) Corner. (d) Noisy corner. (e) Homogeneous. (f) Noisy homogeneous. (g) Squares. (h) Noisy squares.

by [45]

$$\text{ES} = \int g(t - t_0)(EP_{\hat{f}}(t) - EP_X(t))^2 dt \quad (31)$$

where  $g(t - t_0)$  is a Gaussian kernel to assign a larger weight when errors near the edge location  $t_0$  occur. EPs are computed through averaging a homogeneous region in the along-edge direction [45].

FOM quantifies edge preservation based on the output of a detection algorithm. FOM's expression is given by

$$\text{FOM} = \frac{1}{\max(n_d, n_r)} \sum_{i=1}^{n_d} \frac{1}{1 + \gamma d_i^2} \quad (32)$$

where  $n_d$  and  $n_r$  are, respectively, the number of edge pixels detected in the filtered and reference image. The Euclidean distance between the  $i$ th detected edge pixel and the nearest reference edge pixel is represented by  $d_i$ , and  $\gamma$  gives the cost of edge displacement. The range values of FOM is in an interval between 0 and 1. Larger values indicate a superior edge rendition. We apply the same algorithm as in [45], i.e., Canny, to edge detection and  $\gamma = 1/9$  follows the paper selection.

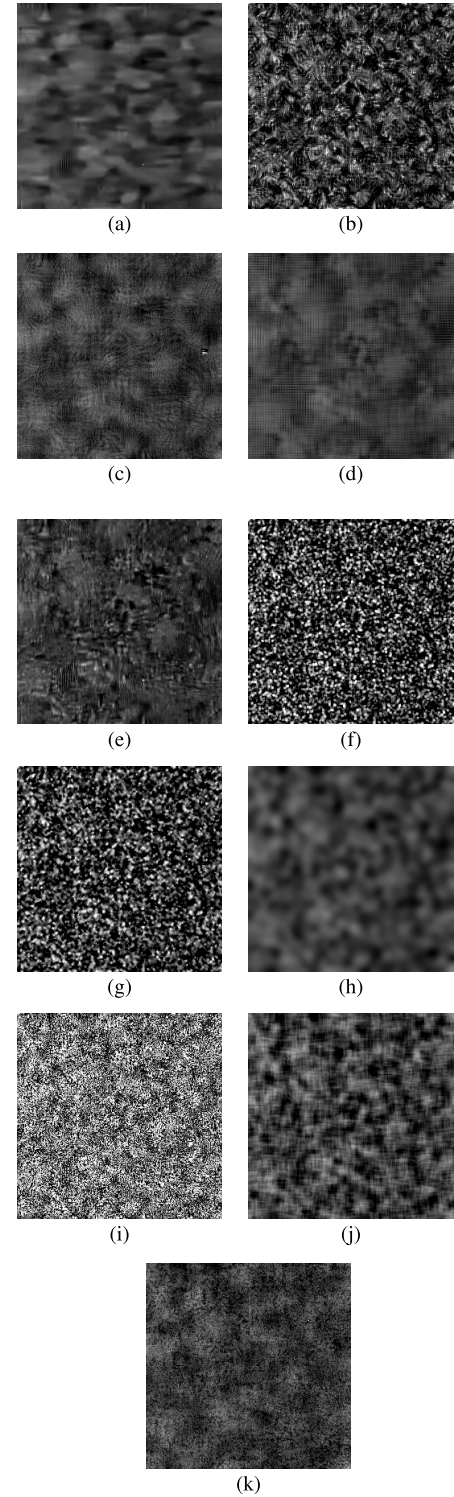


Fig. 7. Results for homogeneous image. PM: proposed method. (a) FANS. (b) OBNLM. (c) PPB. (d) PM. (e) SAR-BM3D. (f) Lee. (g) Frost. (h) NURW. (i) FNLM. (j) NLM-SAP. (k) PNLM.

Table III shows the lower (up) and higher (down) ES contrasts for the two vertical edges. Also, it presents the FOM for the detected edges and time values. Fig. 8 shows the filtered images. Analyzing it, all algorithms tend to produce ES and Fig. 9, which represents the upper edge profiles, emphasizes this statement. Moreover, it shows that our method

TABLE III

VALUES FOR SQUARES' IMAGE. PM: PROPOSED METHOD. VALUES ARE AVERAGES OVER EIGHT SPECKLE REALIZATIONS

	ES (up)	ES (down)	FOM	Time (s)
Clean	-	-	0.99	-
Noisy	0.01	0.02	0.79	-
FANS	0.05	0.15	0.79	12.15
OBNL	0.05	0.13	0.80	1.66
PM	0.09	0.25	0.83	181.95
PPB	0.07	0.20	0.83	87.58
SAR-BM3D	0.03	0.11	0.84	162.52
Lee	0.02	0.07	0.79	0.22
Frost	0.02	0.06	0.80	5.07
NURW	0.14	0.37	0.80	0.53
FNLM	0.09	0.25	0.75	2.47
NLM-SAP	0.12	0.33	0.60	127.84
PNLM	0.25	0.63	0.69	73.94

TABLE IV

VALUES FOR CORNER IMAGE. PM: PROPOSED METHOD. VALUES ARE AVERAGES OVER EIGHT SPECKLE REALIZATIONS

	$C_{NN}$	$C_{BG}$	Time (s)
Clean	7.75	36.56	-
Noisy	7.77	36.50	-
FANS	7.07	35.45	2.37
OBNL	2.28	28.17	0.45
PM	1.19	24.50	19.50
PPB	3.75	32.69	20.49
SAR-BM3D	7.39	35.45	31.01
Lee	-0.32	28.22	0.00
Frost	7.10	35.73	0.95
NURW	2.93	23.31	0.03
FNLM	-0.38	7.18	0.16
NLM-SAP	4.13	20.58	12.78
PNLM	3.58	24.91	9.65

is better than the classical filters and the others with the NLM approach.

The Canny edge detection results in Fig. 10 identifies that all filters, in a certain way, lose some edge details because the edges are not perfectly straight. Together with the FOM values in Table III, it is possible to identify the superiority of the SAR-BM3D and to affirm that the proposed method is competitive with the other filters since it showed an FOM value close to the SAR-BM3D filter.

3) Corner: This image has an artificial corner at the center of a homogeneous scene that gives a high intensity signal return. It is possible to measure the radiometric preservation of the filtered image. Then, two measures are used for the intensity contrast [45]:  $C_{NN}$  and  $C_{BG}$  expressed by

$$C_{NN} = 10 \log_{10} \frac{X_{CF}}{X_{NN}} \quad (33)$$

and

$$C_{BG} = 10 \log_{10} \frac{X_{CF}}{X_{BG}} \quad (34)$$

where  $X_{CF}$  is the average intensity observed in the corner reflector site,  $X_{NN}$  is the average intensity in the surrounding region, and  $X_{BG}$  is the average intensity of the background. A good filter should return values of  $C_{NN}$  and  $C_{BG}$  close enough to the reference image.

From Table IV, we see that the SAR-BM3D maintains its superiority since it has the best  $C_{NN}$  and  $C_{BG}$ . However, in this

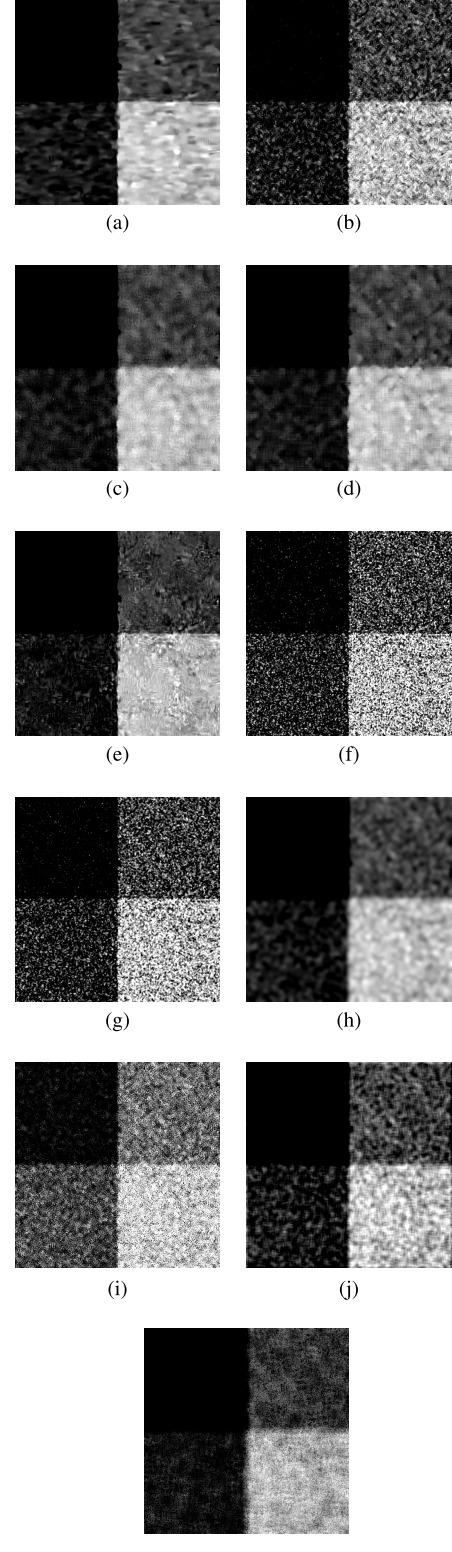


Fig. 8. Results for squares' image. PM: proposed method. (a) FANS. (b) OBNL. (c) PPB. (d) PM. (e) SAR-BM3D. (f) Lee. (g) Frost. (h) NURW. (i) FNLM. (j) NLM-SAP. (k) PNLM.

case, i.e., for single-look speckle noise, it was difficult to draw a conclusion from the measures to identify the superiority of each filter. The Frost algorithm displayed good values in retaining the radiometric aspects of a corner reflector, but its

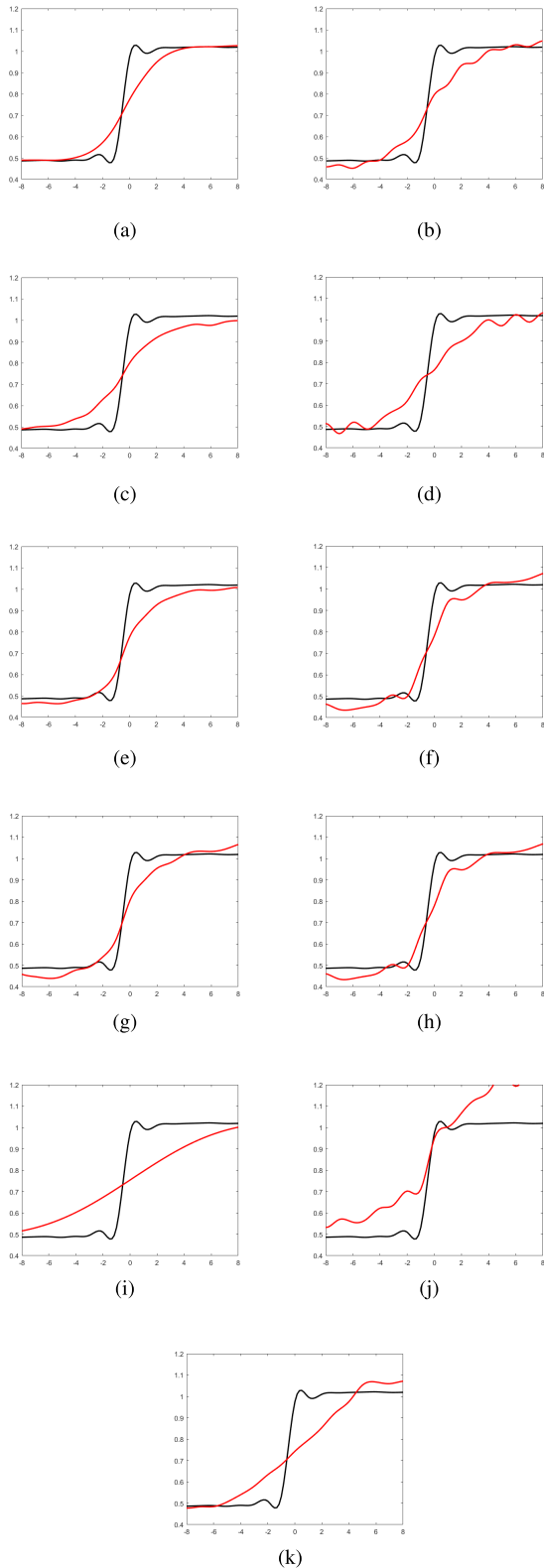


Fig. 9. Results for squares' EPs (upper edge). Red lines: filters' results. Black line: clean image. PM: proposed method. (a) FANS. (b) OBNLM. (c) PPB. (d) PM. (e) SAR-BM3D. (f) Lee. (g) Frost. (h) NURW. (i) FNLM. (j) NLM-SAP. (k) PNLM.

image from Fig. 11 shows that a lot of speckle remains in the surrounding uniform background. This observation also applies to the results of the Lee technique. Furthermore, one

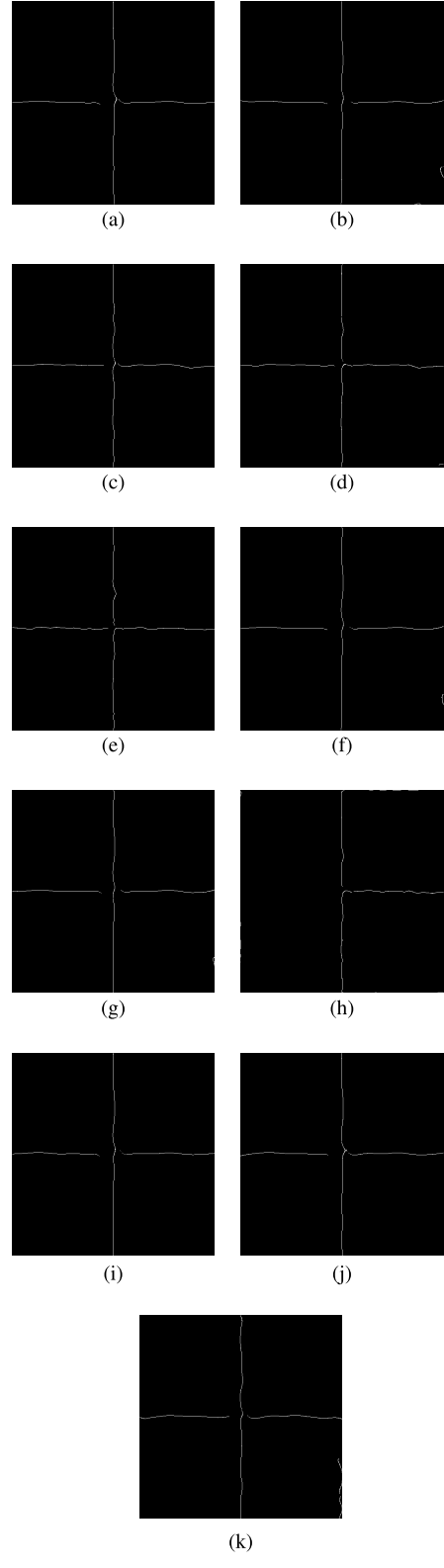


Fig. 10. Results for squares' edge maps with Canny algorithm. PM: proposed method. (a) FANS. (b) OBNLM. (c) PPB. (d) PM. (e) SAR-BM3D. (f) Lee. (g) Frost. (h) NURW. (i) FNLM. (j) NLM-SAP. (k) PNLM.

can say that the proposed method obtained an inferior result by comparing it with some of the other filters. However, the other NLM-based techniques generate oversmoothed images with

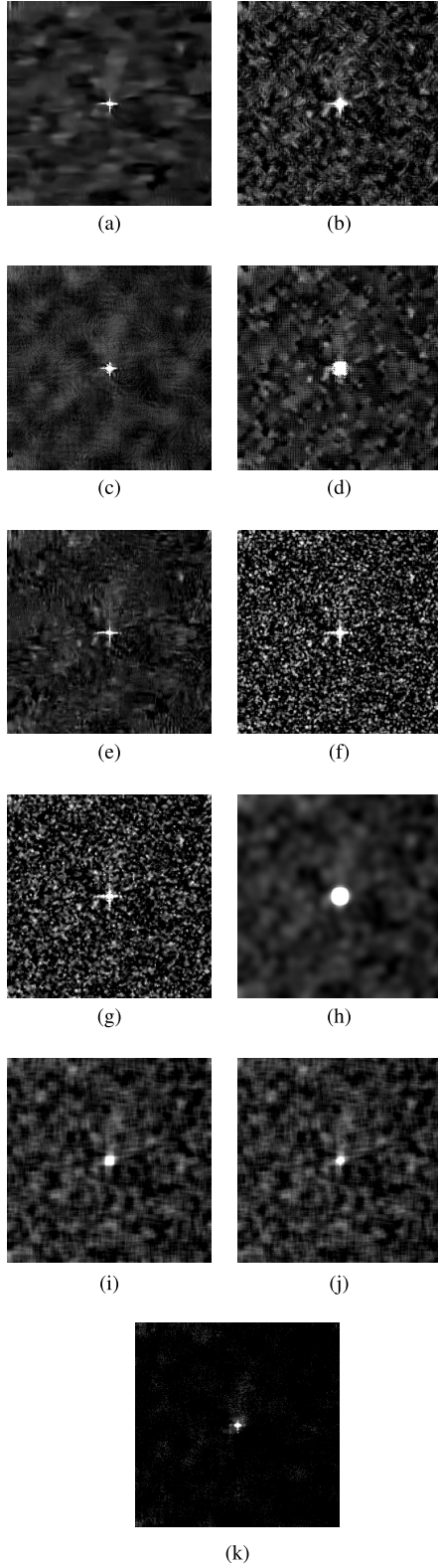


Fig. 11. Results for corner image. PM: proposed method. (a) FANS. (b) OBNLM. (c) PPB. (d) PM. (e) SAR-BM3D. (f) Lee. (g) Frost. (h) NURW. (i) FNLM. (j) NLM-SAP. (k) PNLM.

artifacts, as it is possible to see in the PNLM and NLM-SAP values.

Therefore, the values indicate that a strategy should be investigated for the proposed method to avoid filtering in the

TABLE V  
VALUES FOR BUILDING IMAGE. PM: PROPOSED METHOD. VALUES ARE AVERAGES OVER EIGHT SPECKLE REALIZATIONS

	$C_{DR}$	$BS$	Time (s)
Clean	65.90	-	-
Noisy	65.90	0.09	-
FANS	66.88	3.67	2.34
OBNLM	63.06	15.05	0.32
PM	62.81	15.09	104.07
PPB	64.90	3.13	20.78
SAR-BM3D	65.91	1.46	29.33
Lee	64.01	10.22	0.32
Frost	64.07	12.18	1.26
NURW	58.81	36.23	0.33
FNLM	48.77	14.59	0.30
NLM-SAP	52.96	12.67	14.07
PNLM	53.48	14.35	8.05

corner when it is detected using the Haar wavelet. At the same time, observing the  $C_{NN}$  and  $C_{BG}$  classical and NLM-based filters' values, it is possible to state that these measures favor oversmoothed images. In Fig. 11, it is perceived that PPB and OBNLM not only generate acceptable results but also cause a loss in contrast.

4) Building: The last simulated SAR image has an isolated building over a homogeneous area. This kind of structure presents extreme distortion effects and contributes to emanate the multiple scattering waves. Therefore, the return signal can be a mixture between the neighboring buildings [45]. To analyze the image radiometric precision, we use the contrast expression

$$C_{DR} = 10 \log_{10} \frac{X_{DR}}{X_{BG}} \quad (35)$$

which is the division between the averages' intensity of the double-reflection segment ( $X_{DR}$ ) by the background ( $X_{BG}$ ).

Also, it is possible to use a building smearing (BS) measure [45] to assess the building degradation of the filtered image defined by

$$BS = \int \Pi \left( \frac{t - t_0}{T} \right) | \log_{10}(BP_f(t) + \varepsilon) - \log_{10}(BP_X(t) + \varepsilon) | dt \quad (36)$$

where  $\varepsilon$  is a small positive value and BP is the building profile computed by averaging along the azimuth direction. Both  $C_{DR}$  and BS values must be close to the original image numbers. The proposed filter acts like the building image evaluation. It is clear that a form has to be investigated and applied to prevent the structure filtering when the building is found. Nevertheless, interestingly, it was noticed that all NLM-based filters tend to produce brighter segments around the target edges, which appear by the incorrect filtering of the sidelobes due to the bright double reflection line, and, because of this, they displayed values below Lee and Frost. Table V shows that all algorithms stay close to the original  $C_{DR}$  value. The BS value indicates the good behavior of the SAR-BM3D process. The ratios of the filtered images are shown in Fig. 12. The images confirm the numbers in Table V.

With the synthetic experiments, we tested the filters and pointed out that the proposed algorithm had good results in

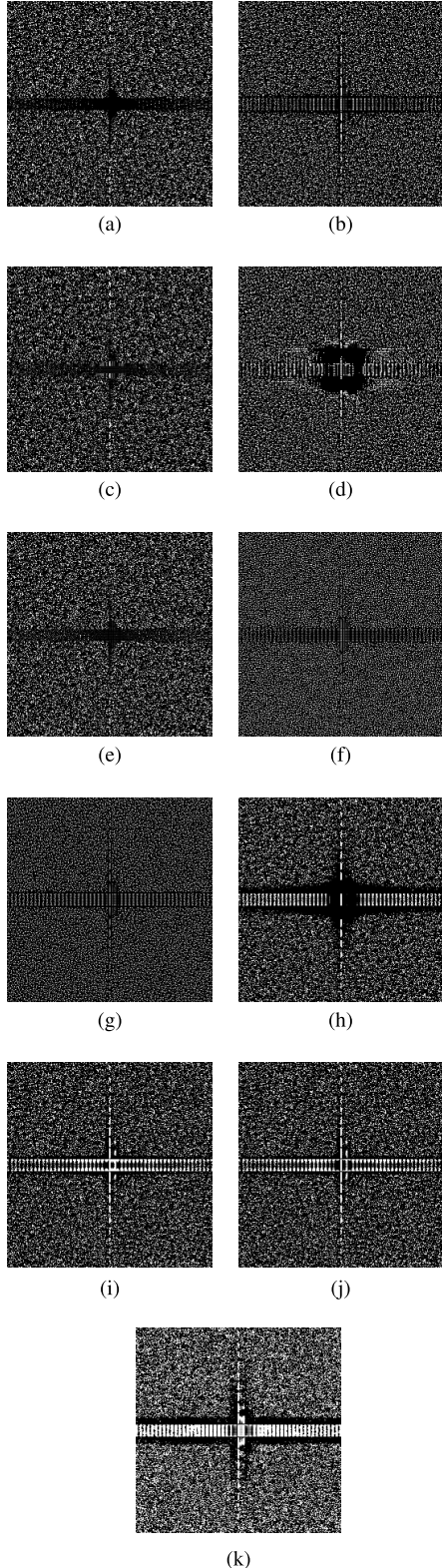


Fig. 12. Results for building image. PM: proposed method. (a) FANS. (b) OBNLM. (c) PPB. (d) PM. (e) SAR-BM3D. (f) Lee. (g) Frost. (h) NURW. (i) FNLM. (j) NLM-SAP. (k) PNLM.

three among four cases. The PM filter, although it has a deficiency of filtering structures in the image, i.e., heterogeneous scenes, obtains good results in homogeneous regions and it is

competitive with other algorithms. The original SAR Benchmark Framework [45] has five case studies. In this paper, the DEM case was not included due to the above-obtained results and the observations about the speckle attenuation deficiency of the proposed filter in heterogeneous images. In the future, if it is possible to describe the EP distribution using another mother wavelet, we may be able to mitigate the speckle in this kind of roughness.

Regarding the NLM parameters' changes, we found a difficulty to find a satisfactory result for each case with the same parameters for the synthetic experiments. This issue clearly needs to be solved in the future work. However, even changing the parameters, the proposed method did not surpass the other filters. It showed that the filter is competitive. Section V-B will indicate that the proposed filter with the stochastic distances has worked well in a real scenario with fixed parameters.

### B. Real Experiments

Three real intensity SAR regions were used to compare and analyze the filters. The Oberpfaffenhofen region near Munich, Germany, is shown in Fig. 13. This is a single-look scene and it was taken through the ESAR platform with an HH polarization. Its dimension is  $7134 \times 1475$ . We chose three random regions with  $512 \times 512$  dimension that contain the most common roughness types: homogeneous, heterogeneous, and extremely heterogeneous. The squares in Fig. 13 indicate these regions. Fig. 14 presents these regions with a better view.

For all regions, the NLM was set with a  $5 \times 5$  patch and an  $11 \times 11$  search window. The approximation coefficient of DWT was filtered with the smoothing parameter  $h = 5 \times 10^{-3}$ . The detail coefficients were processed with  $h = 5 \times 10^{-3} \sigma_{cA}^2$ , where  $\sigma_{cA}^2$  is the approximation coefficient variance. All values were found experimentally. Since it has been seen in the synthetic experiment that the proposed filter was competitive to the classical- and NLM-based ones, we chose to remove them and present the results of OBNLM and PPB.

Examining Figs. 15, 16, and 17, which show the filtered regions 1–3, we can consider that the proposed method is competitive with FANS, PPB, and OBNLM. Visually, the PPB produces blurry images. Furthermore, our approach is quite effective in subtracting the speckle in homogeneous and heterogeneous regions. However, details are lost in extremely heterogeneous surfaces, as described in Section V-A. The FANS filter also removes fine details in heterogeneous areas.

It is not possible to apply the PSNR, SSIM [46], or any other measures that require the original noise-free image since there is no ground truth (noise-free reflectivity). Furthermore, the known equivalent number of looks (ENL) favors over smoothed images, causing a misleading high value [4].

Applying the ratio between the noisy image  $Z$  and the filtered image  $\hat{f}$ :  $r = Z/\hat{f}$  is an effective measure without reference [6]. This ratio shows the standard noise removed that it is supposed to be distributed according to the gamma distribution. With an ideal filter,  $r$  should contain only pure noise pattern. Otherwise, it will give an image with structures and edges [4].

By observing Figs. 18, 19, and 20, we confirm the loss of some structures with our method, such as PPB, OBNLM,



Fig. 13. Oberpfaffenhofen single-look scene.

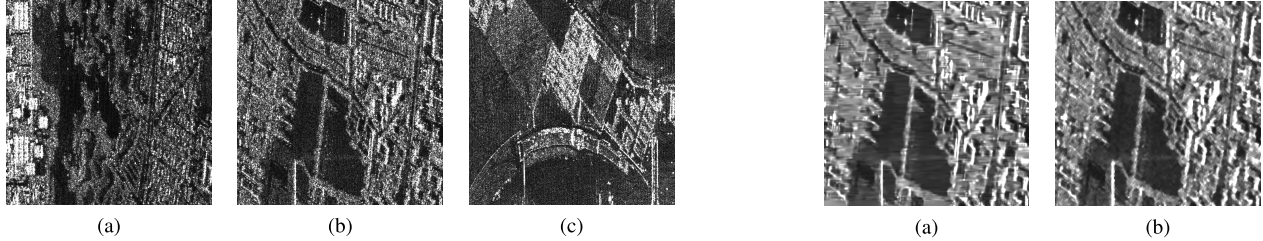
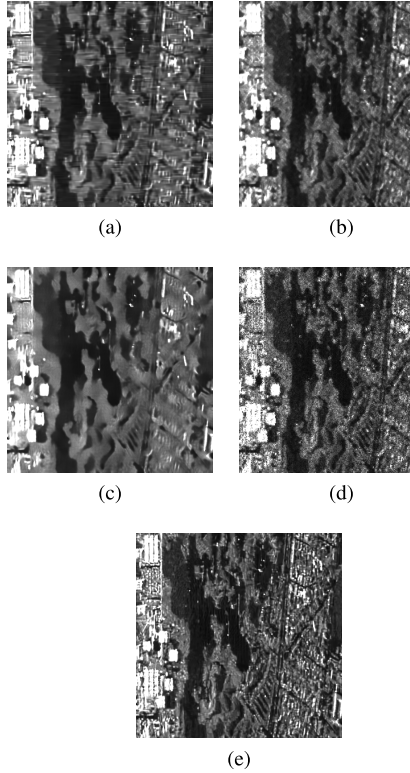
Fig. 14. Intensity HH SAR regions with  $L = 1$ . (a) Region 1. (b) Region 2. (c) Region 3.

Fig. 15. Results for Region 1 (R1). PM: proposed method. (a) FANS. (b) OBNLM. (c) PPB. (d) PM. (e) SAR-BM3D.

and FANS. Although FANS demonstrates good results, it also loses details. The difficulty to find details on the SAR-BM3D ratio confirms its place as the state of the art. Finally, through the real and synthetic results, we can confirm the competitiveness of the proposed filter with the stochastic

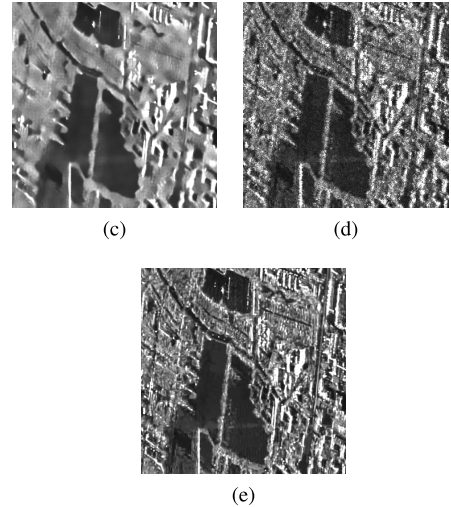


Fig. 16. Results for Region 2 (R2). PM: proposed method. (a) FANS. (b) OBNLM. (c) PPB. (d) PM. (e) SAR-BM3D.

TABLE VI  
MEAN ( $\mu_r$ ) AND VARIANCE ( $\sigma_r$ ) OF REGION 1 RATIO.  
THE BEST RESULTS ARE MARKED IN BOLD

Filters	$\mu_r$	$\sigma_r$	Time (s)
FANS	0.83	0.46	6.43
PM	<b>1.00</b>	<b>0.61</b>	201.03
OBNLM	0.94	0.50	0.97
PPB	0.96	0.57	62.46
SAR-BM3D	0.96	0.42	99.73

distances. The algorithm performs well in homogeneous and heterogeneous regions, although it loses edges in extremely heterogeneous areas.

However, visual inspection can be considered a subjective measure, since it is not possible to detect an introduced bias over the filtered image or to provide a quantitative analysis. According to [4], by using the mean ( $\mu_r$ ) and standard deviation ( $\sigma_r$ ) of the ratio  $r$ , it is possible to make a

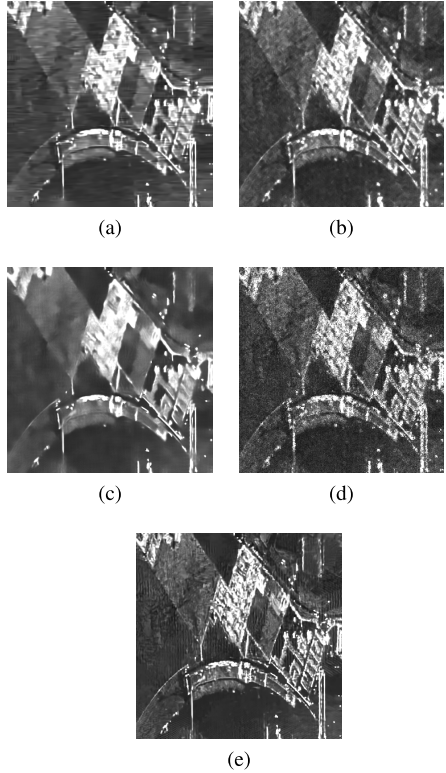


Fig. 17. Results for Region 3 (R3). PM: proposed method. (a) FANS. (b) OBNLM. (c) PPB. (d) PM. (e) SAR-BM3D.

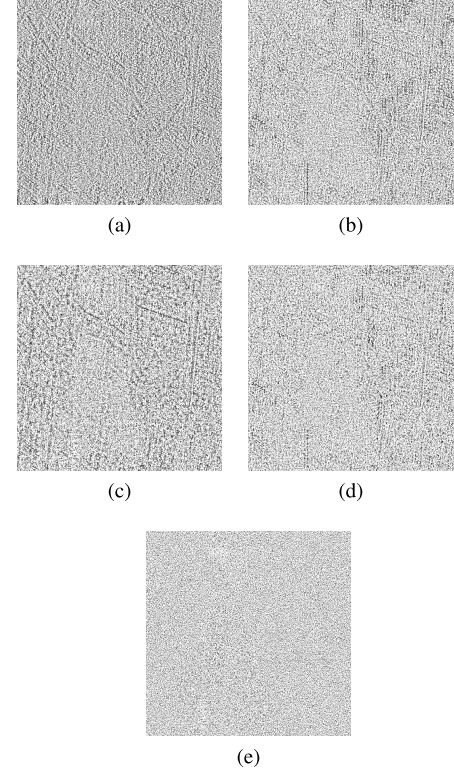


Fig. 19. Ratio for Region 2 (R2). PM: proposed method. (a) FANS. (b) OBNLM. (c) PPB. (d) PM. (e) SAR-BM3D.

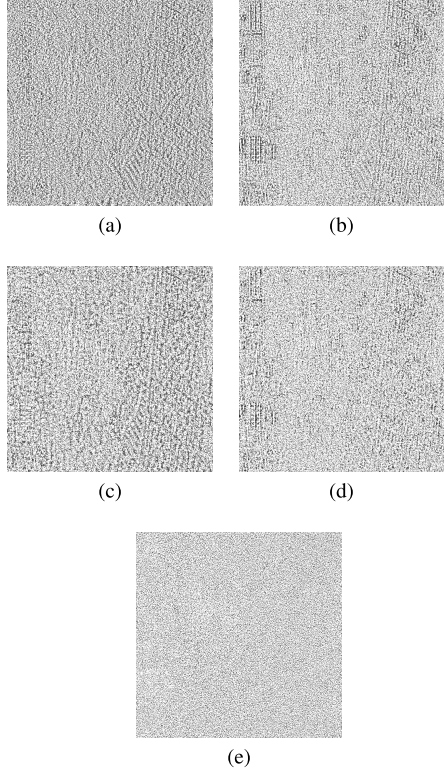


Fig. 18. Ratio for Region 1 (R1). PM: proposed method. (a) FANS. (b) OBNLM. (c) PPB. (d) PM. (e) SAR-BM3D.

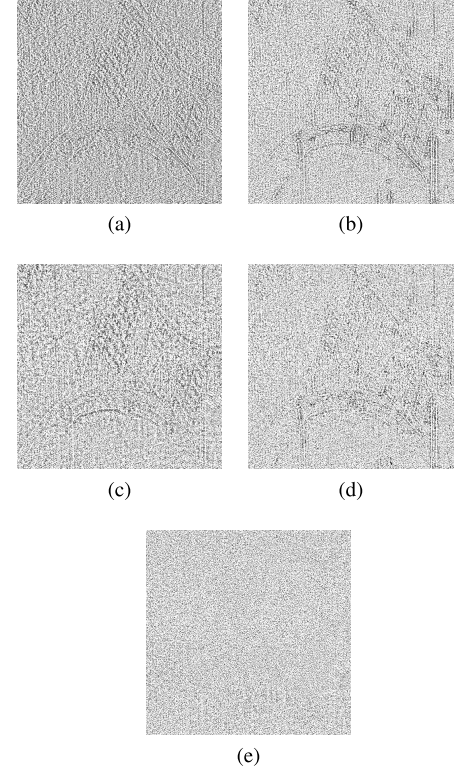


Fig. 20. Ratio for Region 3 (R3). PM: proposed method. (a) FANS. (b) OBNLM. (c) PPB. (d) PM. (e) SAR-BM3D.

quantitative approach. The  $\mu_r$  and  $\sigma_r$  values should be close to the theoretical ones, i.e.,  $\mu \approx 1$  and  $\sigma \approx 1$  for  $L = 1$ .

Tables VI–VIII show the  $\mu_r$  and  $\sigma_r$  values for Regions 1–3. We note that the mean and the variance of the proposed method are the ones that most approached the ideal value. Although the

TABLE VII

MEAN ( $\mu_r$ ) AND VARIANCE ( $\sigma_r$ ) OF REGION 2 RATIO.  
THE BEST RESULTS ARE MARKED IN BOLD

Filters	$\mu_r$	$\sigma_r$	Time (s)
FANS	0.83	0.46	6.83
PM	<b>1.00</b>	<b>1.00</b>	199.57
OBNLM	0.94	0.50	1.10
PPB	0.96	0.57	63.18
SAR-BM3D	0.96	0.44	103.11

TABLE VIII

MEAN ( $\mu_r$ ) AND VARIANCE ( $\sigma_r$ ) OF REGION 3 RATIO.  
THE BEST RESULTS ARE MARKED IN BOLD

Filters	$\mu_r$	$\sigma_r$	Time(s)
FANS	0.84	0.45	6.78
PM	<b>1.00</b>	<b>0.53</b>	200.46
OBNLM	0.96	0.49	1.52
PPB	0.98	<b>0.54</b>	73.14
SAR-BM3D	0.97	0.44	130.32

PPB presents a blurred image, its  $\sigma_r$  is superior to the other algorithms.

## VI. CONCLUSION AND FUTURE WORK

SAR systems are necessary tools to study the surface of the earth. The speckle noise, which appears in SAR images by systems that use coherent imaging, needs to be eliminated. Thereby, a good analysis and interpretation of the scene can be made.

This paper proposed a new technique to filter single-look speckle noise ( $L = 1$ ) in intensity SAR image. It is an approach based on the NLM filter concept, which was originally developed for AWGN noise.

The core of this new approach is to use the stochastic distances calculated for gamma and EP distributions with the NLM algorithm, replacing the Euclidean distance. In addition, the entire filtering process was performed in the domain of the Haar wavelet. The results with the filter and the distances were competitive with the classical filters and the algorithms that also use the NLM philosophy.

The synthetic and real experiments prove that the proposed method is competitive with other recent filters proposed in the literature. It has been proven that the new approach is quite effective at removing the speckle in homogeneous regions. Also, it has been shown that there is a need to circumvent the problem of applying the proposed method in heterogeneous regions. However, the algorithm performance was higher than other filters primarily in removing the speckle in real SAR images.

In addition to innovating through the use of the EP and gamma distributions in the Haar domain, and the corresponding stochastic distances in the NLM filtering, this paper is competitive with the state-of-the-art speckle-filtering algorithms.

Finally, we can cite as a future work to apply the presented stochastic distances with the BM3D algorithm. We can also decrease the execution time of the proposed method by using an optimization of performance or vectorization code for NLM and propose the idea to other wavelets. Also, it is necessary

to solve the loss of details in extremely heterogeneous regions and the parameters' swapping in the synthetic experiments. Furthermore, it is very important to expand the proposed filter to the multilook case, i.e.,  $L > 1$  and to multitemporal or multisensor data set.

## ACKNOWLEDGMENT

The authors would like to thank the researchers for providing the filters' code and also Prof. A. C. Frery for providing the ESAR image.

## REFERENCES

- [1] A. Nath, "Image denoising algorithms: A comparative study of different filtration approaches used in image restoration," in *Proc. Int. Conf. Commun. Syst. Netw. Technol. (CSNT)*, Apr. 2013, pp. 157–163.
- [2] P. Chatterjee and P. Milanfar, "Is denoising dead?" *IEEE Trans. Image Process.*, vol. 19, no. 4, pp. 895–911, Apr. 2010.
- [3] C.-A. Deledalle, L. Denis, S. Tabti, and F. Tupin, "MuLoG, or how to apply Gaussian denoisers to multi-channel SAR speckle reduction?" *IEEE Trans. Image Process.*, vol. 26, no. 9, pp. 4389–4403, Sep. 2017.
- [4] P. A. Penna and N. D. A. Mascarenhas, "(Non-) homomorphic approaches to denoise intensity SAR images with non-local means and stochastic distances," *Comput. Geosci.*, vol. 111, pp. 127–138, Feb. 2018. [Online]. Available: <http://www.sciencedirect.com/science/article/pii/S0098300417300432>
- [5] S. Parrilli, M. Poderico, C. V. Angelino, and L. Verdoliva, "A nonlocal SAR image denoising algorithm based on LLMMSE wavelet shrinkage," *IEEE Trans. Geosci. Remote Sens.*, vol. 50, no. 2, pp. 606–616, Feb. 2012.
- [6] F. Argenti, A. Lapini, T. Bianchi, and L. Alparone, "A tutorial on speckle reduction in synthetic aperture radar images," *IEEE Geosci. Remote Sens. Mag.*, vol. 1, no. 3, pp. 6–35, Sep. 2013.
- [7] H. H. Arsenault and G. April, "Properties of speckle integrated with a finite aperture and logarithmically transformed," *J. Opt. Soc. Amer.*, vol. 66, no. 11, pp. 1160–1163, Nov. 1976. [Online]. Available: <http://www.osapublishing.org/abstract.cfm?URI=josa-66-11-1160>
- [8] A. Buades, B. Coll, and J. M. Morel, "A review of image denoising algorithms, with a new one," *Multiscale Model. Simul.*, vol. 4, no. 2, pp. 490–530, 2005.
- [9] K. Dabov, A. Foi, V. Katkovnik, and K. Egiazarian, "Image denoising by sparse 3-D transform-domain collaborative filtering," *IEEE Trans. Image Process.*, vol. 16, no. 8, pp. 2080–2095, Aug. 2007.
- [10] M. Aharon, M. Elad, and A. Bruckstein, "K-SVD: An algorithm for designing overcomplete dictionaries for sparse representation," *IEEE Trans. Signal Process.*, vol. 54, no. 11, pp. 4311–4322, Nov. 2006.
- [11] A. A. Efros and T. K. Leung, "Texture synthesis by non-parametric sampling," in *Proc. IEEE Int. Conf. Comput. Vis.*, vol. 2, Sep. 1999, pp. 1033–1038.
- [12] C.-A. Deledalle, L. Denis, and F. Tupin, "Iterative weighted maximum likelihood denoising with probabilistic patch-based weights," *IEEE Trans. Image Process.*, vol. 18, no. 12, pp. 2661–2672, Dec. 2009.
- [13] T. Teuber and A. Lang, "A new similarity measure for nonlocal filtering in the presence of multiplicative noise," *Comput. Statist. Data Anal.*, vol. 56, no. 12, pp. 3821–3842, 2012.
- [14] C.-A. Deledalle, L. Denis, F. Tupin, A. Reigber, and M. Jäger, "NL-SAR: A unified nonlocal framework for resolution-preserving (Pol)In) SAR denoising," *IEEE Trans. Geosci. Remote Sens.*, vol. 53, no. 4, pp. 2021–2038, Apr. 2015.
- [15] G. D. Martino, A. Di Simone, A. Iodice, and D. Riccio, "Scattering-based nonlocal means SAR despeckling," *IEEE Trans. Geosci. Remote Sens.*, vol. 54, no. 6, pp. 3574–3588, Jun. 2016.
- [16] X. Nie, X. Huang, and W. Feng, "A new nonlocal TV-based variational model for SAR image despeckling based on the G0 distribution," *Digit. Signal Process.*, vol. 68, pp. 44–56, Sep. 2017. [Online]. Available: <http://www.sciencedirect.com/science/article/pii/S1051200417300982>
- [17] D. Cozzolino, S. Parrilli, G. Scarpa, G. Poggi, and L. Verdoliva, "Fast adaptive nonlocal SAR despeckling," *IEEE Geosci. Remote Sens. Lett.*, vol. 11, no. 2, pp. 524–528, Feb. 2014.
- [18] A. D. C. Nascimento, R. J. Cintra, and A. C. Frery, "Hypothesis testing in speckled data with stochastic distances," *IEEE Trans. Geosci. Remote Sens.*, vol. 48, no. 1, pp. 373–385, Jan. 2010.

- [19] L. Torres, T. Cavalcante, and A. C. Frery, "Speckle reduction using stochastic distances," in *Progress in Pattern Recognition, Image Analysis, Computer Vision, and Applications* (Lecture Notes in Computer Science), vol. 7441, L. Alvarez, M. Mejail, L. Gomez, and J. Jacobo, Eds. Berlin, Germany: Springer, 2012, pp. 632–639.
- [20] L. Torres and A. C. Frery, "SAR image despeckling algorithms using stochastic distances and nonlocal means," in *Proc. Workshop 26th Conf. Graph, Patterns Images (WTD) SIBGRAPI*, Arequipa, Peru, Aug. 2013, pp. 1–6.
- [21] L. Torres, S. J. Sant'Anna, C. da Costa Freitas, and A. C. Frery, "Speckle reduction in polarimetric SAR imagery with stochastic distances and nonlocal means," *Pattern Recognit.*, vol. 47, no. 1, pp. 141–157, 2014. [Online]. Available: <http://www.sciencedirect.com/science/article/pii/S0031320313001532>
- [22] C. A. N. Santos, D. L. N. Martins, and N. D. A. Mascarenhas, "Ultrasound image despeckling using stochastic distance-based BM3D," *IEEE Trans. Image Process.*, vol. 26, no. 6, pp. 2632–2643, Jun. 2017.
- [23] C. A. N. Santos and N. D. A. Mascarenhas, "Geodesic distances in probabilistic spaces for patch-based ultrasound image processing," *IEEE Trans. Image Process.*, vol. 28, no. 1, pp. 216–226, Jan. 2019.
- [24] C. A. N. Santos and N. D. A. Mascarenhas, "Patch similarity in ultrasound images with hypothesis testing and stochastic distances," *Comput. Med. Imag. Graph.*, vol. 74, pp. 37–48, Jun. 2019. [Online]. Available: <http://www.sciencedirect.com/science/article/pii/S089561111930028X>
- [25] A. A. Bindilatti and N. D. A. Mascarenhas, "A nonlocal Poisson denoising algorithm based on stochastic distances," *IEEE Signal Process. Lett.*, vol. 20, no. 11, pp. 1010–1013, Nov. 2013.
- [26] A. A. Bindilatti, M. A. C. Vieira, and N. D. A. Mascarenhas, "Poisson Wiener filtering with non-local weighted parameter estimation using stochastic distances," *Signal Process.*, vol. 144, pp. 68–76, Mar. 2018. [Online]. Available: <http://www.sciencedirect.com/science/article/pii/S0165168417303523>
- [27] S. G. Mallat, "A theory for multiresolution signal decomposition: The wavelet representation," *IEEE Trans. Pattern Anal. Mach. Intell.*, vol. 11, no. 7, pp. 674–693, Jul. 1989.
- [28] R. S. Stankovic and B. J. Falkowski, "The Haar wavelet transform: Its status and achievements," *Comput. Elect. Eng.*, vol. 29, no. 1, pp. 25–44, 2003. [Online]. Available: <http://www.sciencedirect.com/science/article/pii/S0045790601000118>
- [29] A. Misra, B. Kartikeyan, and S. Garg, "Wavelet based SAR data denoising and analysis," in *Proc. IEEE Int. Adv. Comput. Conf. (IACC)*, Feb. 2014, pp. 1087–1092.
- [30] A. K. Chan and C. Peng, *Wavelets for Sensing Technologies*. Boston, MA, USA: Artech House, 2003.
- [31] J.-S. Lee, "Digital image enhancement and noise filtering by use of local statistics," *IEEE Trans. Pattern Anal. Mach. Intell.*, vol. PAMI-2, no. 2, pp. 165–168, Feb. 1980.
- [32] V. S. Frost, J. A. Stiles, K. S. Shanmugan, and J. C. Holtzman, "A model for radar images and its application to adaptive digital filtering of multiplicative noise," *IEEE Trans. Pattern Anal. Mach. Intell.*, vol. PAMI-4, no. 2, pp. 157–166, Mar. 1982.
- [33] S.-S. Jiang and A. A. Sawchuk, "Noise updating repeated Wiener filter and other adaptive noise smoothing filters using local image statistics," *Appl. Opt.*, vol. 25, no. 14, pp. 2326–2337, Jul. 1986. [Online]. Available: <http://ao.osa.org/abstract.cfm?URI=ao-25-14-2326>
- [34] J. W. Goodman, "Some fundamental properties of speckle," *J. Opt. Soc. Amer.*, vol. 66, no. 11, pp. 1145–1150, Nov. 1976. [Online]. Available: <http://www.osapublishing.org/abstract.cfm?URI=josa-66-11-1145>
- [35] J. Zhang, G. Lin, L. Wu, C. Wang, and Y. Cheng, "Wavelet and fast bilateral filter based de-speckling method for medical ultrasound images," *Biomed. Signal Process. Control*, vol. 18, pp. 1–10, Apr. 2015. [Online]. Available: <http://www.sciencedirect.com/science/article/pii/S1746809414001955>
- [36] E. S. Ribeiro, "Portuguese novas propostas em filtragem de projeções tomográficas sob ruído Poisson," M.S. thesis, Dept. Comput., Federal Univ. São Carlos, São Carlos, Brazil 2010.
- [37] B. Klar, "A note on gamma difference distributions," *J. Stat. Comput. Simul.*, vol. 85, no. 18, pp. 3708–3715, 2015. [Online]. Available: <http://dx.doi.org/10.1080/00949655.2014.996566>
- [38] E. Krishna and K. K. Jose, "Marshall-Olkin generalized asymmetric Laplace distributions and processes," *Statistica*, vol. 71, no. 4, pp. 453–467, 2011. [Online]. Available: <https://rivista-statistica.unibo.it/article/view/3627>
- [39] M. Salicrú, D. Morales, M. L. Menéndez, and L. Pardo, "On the applications of divergence type measures in testing statistical hypotheses," *J. Multivariate Anal.*, vol. 51, no. 2, pp. 372–391, 1994. [Online]. Available: <http://www.sciencedirect.com/science/article/pii/S0047259X84710682>
- [40] *MATLAB Version 9.0.0.341360 (R2016a)*, MathWorks, Natick, MA, USA, 2016.
- [41] P. Coupé, P. Hellier, C. Kervrann, and C. Barillot, "Nonlocal means-based speckle filtering for ultrasound images," *IEEE Trans. Image Process.*, vol. 18, no. 10, pp. 2221–2229, Oct. 2009.
- [42] J. Darbon, A. Cunha, T. Chan, S. Osher, and G. Jensen, "Fast nonlocal filtering applied to electron cryomicroscopy," in *Proc. 5th IEEE Int. Symp. Biomed. Imag., From Nano Macro (ISBI)*, May 2008, pp. 1331–1334.
- [43] Y. Wu, B. Tracey, P. Natarajan, and J. P. Noonan, "Probabilistic non-local means," *IEEE Signal Process. Lett.*, vol. 20, no. 8, pp. 763–766, Aug. 2013.
- [44] C. A. Deledalle, V. Duval, and J. Salmon, "Non-local methods with shape-adaptive patches (NLM-SAP)," *J. Math. Imag. Vis.*, vol. 43, no. 2, pp. 103–120, Jun. 2012.
- [45] G. Di Martino, M. Poderico, G. Poggi, D. Riccio, and L. Verdoliva, "Benchmarking framework for SAR despeckling," *IEEE Trans. Geosci. Remote Sens.*, vol. 52, no. 3, pp. 1596–1615, Mar. 2014.
- [46] Z. Wang, A. C. Bovik, H. R. Sheikh, and E. P. Simoncelli, "Image quality assessment: From error visibility to structural similarity," *IEEE Trans. Image Process.*, vol. 13, no. 4, pp. 600–612, Apr. 2004.